https://doi.org/10.3311/PPCi.36877

Periodica Polytechnica Civil Engineering, 68(4), pp. 1243–1254, 2024

Estimation of Bond Strength based on Corroded Hinge Beam Specimens: Assessment of Design Guidelines and Analytical Models

Bharat Bhushan[1], Harish Chandra Arora[2,3], Aman Kumar[2,3*], Prashant Kumar[2,3], Surabhi Sharma[1], Madhu Sharma[4]

[1] Department of Civil Engineering, Jawaharlal Nehru Government Engineering College, 175018 Sundernagar, India
[2] Structural Engineering Department, CSIR-Central Building Research Institute, 247667 Roorkee, India
[3] Academy of Scientific and Innovative Research (AcSIR), 201002 Ghaziabad, India
[4] Civil Engineering Department, Government Hydro Engineering College, 174001 Bilaspur, India
[*] Corresponding author, e-mail: aman.civil17@gmail.com

Received: 14 March 2024, Accepted: 28 April 2024, Published online: 27 June 2024

Abstract

The bond between steel and concrete enhances the structural integrity of the building and ensures a cohesive force-resistant system, facilitating composite action between the rebars and concrete. This composite action, in turn, ensures the longevity of the reinforced concrete (RC) structure. The current study focuses on evaluating the performance and comparing design guidelines and analytical models pertaining to hinge beams and pull-out test specimens. The bond strength between concrete and steel was determined by validating 124 experimental datasets collected from the literature. These datasets were based on hinge and pocket beam specimens with varying degrees of corrosion. To facilitate comparison, the international design guidelines and analytical models were designated as G-1 and G-2, respectively. The results indicate that Model M-6 from G-1 and Model M-10 from G-2 outperformed all other models within their respective groups. Upon comparing these two models, M-6 appears to be superior based on selected performance indices. Model M-6 demonstrated an R-value of 0.3275, MAE of 2.29 MPa, RMSE of 2.76 MPa, and MAPE of 39.12% sequentially. Additionally, sensitivity analysis based on the collected dataset was conducted to assess the impact of each parameter.

This study offers a comprehensive analysis of bond strength between steel and concrete in RC structures, focusing on hinge beams and pull-out test specimens with varying degrees of corrosion. It introduces superior models for performance evaluation and comparative analysis, highlighting Model M-6 as a novel and robust approach with significant potential for enhancing structural design guidelines.

Keywords

corrosion, bond strength, steel-to-concrete, structural integrity, hinge beam, pocket beam

1 Introduction

Reinforced concrete (RC) structures, owing to their remarkable strength and durability, form the backbone of modern infrastructure [1]. However, a critical challenge that threatens their serviceability and longevity is corrosion. Corrosion occurs when the reinforcing steel within the concrete starts to deteriorate due to environmental factors such as moisture, oxygen, and chemical ingress. This process leads to the formation of rust, which weakens both the concrete and the steel reinforcement. It is similar to the gradual decay is observed when metal objects are exposed to the elements over time [2, 3].

The corrosion of reinforcing steel can be attributed to various factors, including the presence of chlorides, carbonation of concrete, and the breakdown of protective layers. Chlorides, commonly found in seawater or deicing salts, can penetrate the concrete and trigger the corrosion process. Similarly, carbonation occurs when carbon dioxide from the atmosphere reacts with the alkaline components in concrete, lowering the pH levels and compromising the passivity of the steel reinforcement. Consequently, the protective oxide film on the steel surface breaks down, rendering it susceptible to corrosion initiation and propagation [4].

Corrosion can have a detrimental impact on the bond strength (BS) between reinforcing elements and concrete in structures, leading to significant structural deterioration.

Cite this article as: Bhushan, B., Arora, H. C., Kumar, A., Kumar, P., Sharma, S., Sharma, M. "Estimation of Bond Strength based on Corroded Hinge Beam Specimens: Assessment of Design Guidelines and Analytical Models", Periodica Polytechnica Civil Engineering, 68(4), pp. 1243–1254, 2024. https://doi.org/10.3311/PPCi.36877

When steel reinforcement corrodes, it undergoes a volumetric expansion, causing localized stress concentrations and ultimately leading to cracking and spalling of the concrete cover. This compromised concrete cover exposes the reinforcement to further corrosion, creating a vicious cycle of degradation. As corrosion progresses, the bond between the corroded reinforcement and the surrounding concrete weakens, reducing the structural integrity of the member. In severe cases, the BS can be severely compromised, reducing the load-carrying capacity of the structure and posing a safety risk. Furthermore, the loss of BS can accelerate the progression of corrosion, exacerbating the structural damage and potentially leading to structural failure if not addressed promptly and effectively. Thus, corrosion-induced deterioration of BS represents a critical concern in the maintenance and rehabilitation of RC structures [4, 5].

One crucial aspect in ensuring the structural integrity of RC constructions is the BS between the concrete matrix and the embedded reinforcement. A strong bond facilitates efficient stress transfer between the concrete and the steel, thereby enhancing the overall performance of the structure under load. Consequently, assessing and understanding this BS is paramount in designing and maintaining resilient RC structures [5].

Traditionally, researchers have relied on pull-out tests to evaluate the BS between concrete and steel. In this test, a steel bar is embedded in concrete, and then an attempt is made to pull it out. The force required to extract the bar provides an indication of the BS. However, this method has limitations, as it does not fully replicate real-world loading conditions. In the pull-out test, the concrete surrounding the bar is subjected to compression while the bar itself experiences tension. This discrepancy can result in inaccurate estimations of the BS [6].

To address this limitation, researchers have developed alternative methods such as the hinge beam test (HBT). The HBT simulates more realistic loading conditions by subjecting both the concrete and the embedded steel reinforcement to tension. This setup closely resembles the actual behavior of RC structures under load, providing more accurate insights into the BS [7]. The corrosion effect on BS is generally investigated by the pull-out test [8–12] and the HBT along with the pocket beam test [7, 13–17]. The test results may vary due to differences in test methods and loading conditions but a common result can be attained that the BS first increases with little corrosion and then decreases as the corrosion intensity increases [7]. Ma et al. [3] examined the bond between bars and the concrete by using a pull-out test and concluded that corrosion effects on deformed bars were less as compared to plain bars. Choi et al. [12] examined the impact of corrosion on bond deterioration in RC specimens. They observed that as corrosion exceeded 5%, slip at the failure section increased. Conversely, when corrosion levels dropped below 1%, the BS increased. Notably, a 50% increase in corrosion led to instances of brittle failure. Hou et al. [18] developed a model for estimating BS through pull-out testing and concluded that the variation in BS with corrosion ratio correlates with embedment length. Shang et al. [16] emphasized that the corrosion process of steel bars was expedited under sustained load, leading to the formation of initial cracks and the generation of new ones. Therefore, it is essential to consider the influence of loading when investigating the bond behavior between corroded steel bars and concrete. Chai et al. [7] performed HBT with varying corrosion intensities and various sustained loading for determining BS. The results suggest that both load and corrosion significantly impact the slip and BS between the concrete and steel bar. Corrosion levels below 1% results in higher BS, reaching up to 1.22 times that of uncorroded specimens, while corrosion more than 2.4% leads to a lowering of BS. Shang and Chai [17] performed HBT and also concluded that BS first increases and than decreases. Researchers also concluded that at higher corrosion rate, higher will be the slip. This is because corrosion weakens the bonding force by crushing of concrete present in between the lugs/ribs, which makes the pulling out the steel bar out of the concrete easier. Lin and Zhao [13] studied the effect of corrosion on the lateral confinement and concluded that the stirrups can limit the cracking of the concrete cover and increase the BS of corroded steel bars. The skeleton diagram of the hinge and pocket beams is shown in Figs. 1 and 2, respectively.

Apart from that various researchers have discussed the BS related to fibre-reinforced polymers (FRP) using machine learning (ML). Shbeeb et al. [19] employed artificial neural networks (ANN) and adaptive neuro-fuzzy inference system (ANFIS) to predict FRP-concrete bond behavior using 238 data points from various literature

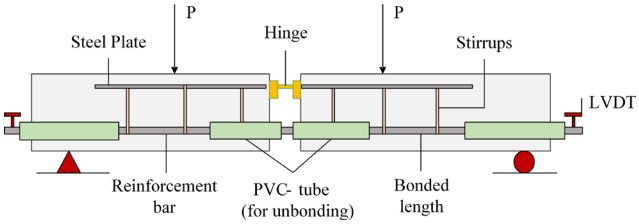

Fig. 1 Hinge beam

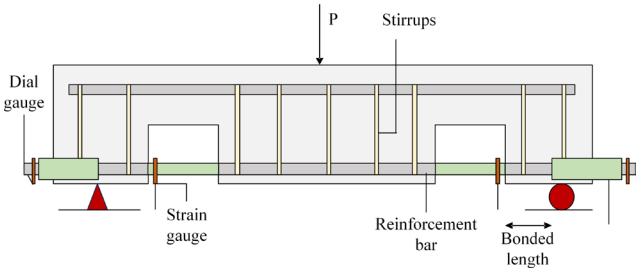

Fig. 2 Pocket beam

sources. The results indicated superior prediction performance of both the models. For instance, the R^2 values for ANN and ANFIS were 0.94 and 0.92, respectively. Sensitivity analysis identified FRP diameter and concrete compressive strength as the most influential parameters on BS in both models. Jahangir et al. [20] employed textile-reinforced mortar (TRM) in place of FRP for the determination of BS by considering a database of 221. A new TRM model was calibrated by implementing soft computing techniques which shows higher accuracy with an R-value of 0.69. Al-Hamd et al. [21] determined BS between FRP and concrete using soft computing techniques such as gene expression programming (GEP) and multi-objective genetic algorithm evolutionary polynomial regression (MOGA-EPR). The results showed the efficient performance of both the models having R^2 values of 0.91 and 0.94, respectively. Jahangir et al. [22] employed steel reinforced polymer (SRP) in place of FRP for determining BS. The authors investigated bond behavior with different bond lengths and widths. Failure mode and range of effective bonded length were evaluated. Also, a new model was proposed to determine SRP-concrete BS. Jahangir and Rezazadeh Eidgahee [23] determined BS between FRP strip and concrete using ML. ANN with a combination of ABC-ANN was implemented for model development. The results of the developed models were compared with existing models and design guidelines. In comparison, the developed models exhibit superior performance, achieving R values of 0.97 and 0.93 for ABC-ANN and ANN, respectively. Jahangir and Esfahani [24] performed an empirical investigation for steel reinforced grout (SRG) composite-concrete interface. Analysis of load response revealed that the load responses were affected by loading rate, fiber density as well as load response measurement variable. Also, the out of plane displacement increases with higher loading rates and is independent of specimen density. Jahangir et al. [25] investigated short concrete columns with square cross-section having confinement of steel fiber and grout composites named SRP and SRG composites. The comparison between confined and unconfined samples was done on the basis of loading capacity and ultimate strain. From the results, it was concluded that the general failure mode of SRP and SRG-confined concrete columns was the detachment of overlapping surfaces. The average compressive strength and strain at maximum load were noted at 7.9% and 9.8%, respectively.

2 Objective of the study

The study's main focus is to assess the effectiveness of international design guidelines and analytical models to determine the bond strength (BS) between steel and concrete. The performance of the international design guidelines and analytical models has been checked using commonly used performance indices such as R, MAPE, MAE, RMSE, NS, and a20-index. Based on the performance indices the best international design guideline and an analytical model is suggested.

3 Research significance

Limited experimental work has been done on determining the BS with the help of HBT. Recognizing HBT's superior results compared to pull-out testing, there is a need to establish the BS through beam testing specimens. However, this process demands significant manpower, resources, and time. Therefore, this study addresses this challenge by adopting a data-driven approach, collecting information from existing literature on HBT and pocket beam specimens to ascertain the BS within rebars and concrete. Assessing design guidelines and analytical models using experimental data holds significant importance in the field of structural engineering. This process allows the validation and refinement of existing design guidelines and models, ensuring their accuracy and applicability in real-world scenarios. Improved accuracy in analytical models enables engineers to develop more precise and efficient structural designs, reducing the risk of failure and enhancing overall safety. Notably, no prior researcher has applied a data-driven approach to validate the existing BS models based on HBT, making this study significant in multiple aspects as discussed above.

4 Experimental data and working methodology

This study involves a data-driven approach by collecting a database on BS based on HBT [7, 15–17] and pocket beams [13, 14] from the literature. Additionally, analytical models given in previous studies based on beam testing and the pull-out testing were also considered for making

comparison using performance indices. The working methodology of work is shown in Fig. 3.

4.1 Summary of collected dataset

This study consists of 124 experimental datasets that were gathered from published literature. The dataset consists of both plain and deformed bars and no other type of bars other than steel bars were considered [7, 13–17]. A brief description of the dataset is given in Table A1 (Appendix A). The considered input parameters were cover of concrete (c), diameter of bar (d_b), type of rebar (t_b), embedded length (l_b), compressive strength of concrete (f_c'), yielding capacity of bar (f_y), corrosion level (η), stirrups spacing (S_v) and stirrups diameter (S_d) for prediction of BS (τ_u). BS ranges from 2.98–14.92 MPa and corrosion ranges between 0.08–20.86%. In the majority of experimental dataset, the f_c' was around 30 MPa. The value of embedded bar length ranges between 70–150 mm, with diameter ranges between 10–20 mm. The yield strength of the bar varies from 357.5–540 MPa, and the range of cover was between 20–40 mm.

4.2 Evaluation of data

The effectiveness of analytical models and design guidelines was evaluated using six performance indices as mentioned in Table 1 [26–28].

The provided expression represents a metric for evaluating the relationship between experimental (ei) and predicted (pi) sets where e' and p' are the mean of experimental and predicted values, respectively. N shows the number of data points, and $m20$ represents the count of values falling between 0.8 to 1.2 when experimental values are divided by predicted values.

5 Design guidelines and analytical models

Six design guidelines and six analytical models were employed in the present study to compare the performance of the models. The model assigned (1–12) were CEB-FIP [29], FIB model code 2010 [30], AS-3600 [31], ACI 408R-03 [32], Stanish et al. [33], Orangun et al. [34], Darwin et al. [35], Esfahani and Rangan [36], Siempu and Pancharthi [37], Harajli [38], termed as M1–M12 in this study. The description of these models along with performance is given in Table 2 [29–38].

6 Results and discussion

In this study, six international design guidelines and analytical models were selected to assess their performance. The international design guidelines utilized in this study were designated as Group-1 (G-1). Additionally,

Table 1 Performance indices

Parameter	Expression	Ideal value
R	$\frac{\sum_{i=1}^{N}(ei-e')(pi-p')}{\sqrt{\sum_{i=1}^{N}(ei-e')^2\sum_{i=1}^{N}(pi-p')^2}}$	1
MAE	$\frac{1}{N}\sum_{i=1}^{N}\lvert ei-pi\rvert$	0
MAPE	$\frac{1}{N}\sum_{i=1}^{N}\left\lvert\frac{ei-pi}{ei}\right\rvert\times 100$	0
RMSE	$\sqrt{\frac{1}{N}\sum_{i=1}^{N}(ei-pi)^2}$	0
NS	$1-\frac{\sum_{i=1}^{N}(ei-pi)^2}{\sum_{i=1}^{N}(ei-p')^2}$	1
a20-index	$\frac{m20}{N}$	1

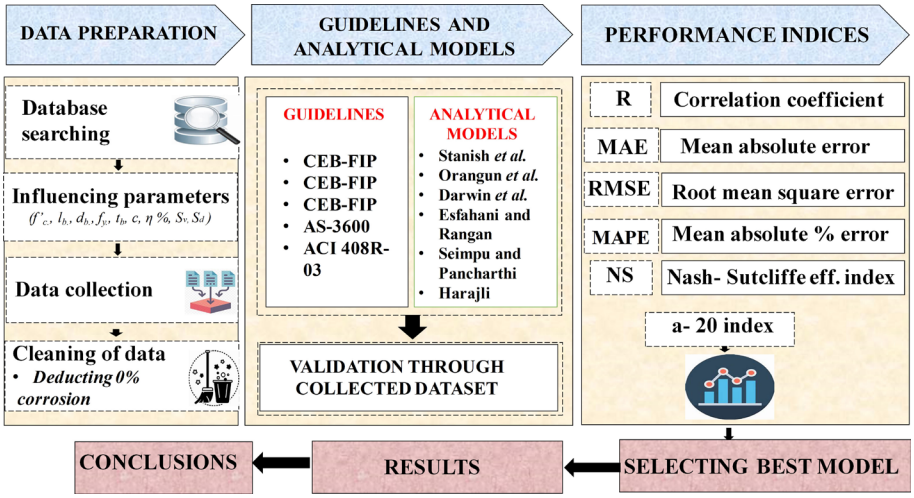

Fig. 3 Working methodology

Table 2 Description of design guidelines and analytical models

Model	Formulation	Remarks	Units
M-1 [29]	$\tau_u = 13.5\sqrt{f_c'/30}$	τ_u = bond strength f_c' = compressive strength	S.I.
M-2 [29]	$\tau_u = 7.0\left(\sqrt{f_c'/25}\right)^{0.25}$		
M-3 [30]	$\tau_u = 2.5\sqrt{f_c'}$		
M-4 [31]	$\tau_u = 0.265\sqrt{f_c'}\left[\frac{c}{d_b} + 0.5\right]$	c = minimum cover d_b = diameter of bar	
M-5 [32]	$\tau_{\max} = \left\{\left(9.53 + 19.07\left(\frac{c_{\min}}{d}\right) + 600\left(\frac{d}{l}\right)\left(0.9 + 0.1\left(\frac{c_{\max}}{c_{\min}}\right)\right)\right)\right\} f_{cy}^{1/4}$	$\tau_{\max}$ = bond strength, $c_{\min}$ = min. cover, f_{cy} = cylindrical compressive strength, $c_{\max}$ = max. cover, l = embedded length	PSI
M-6 [30]	$\tau_u = 7.0 \times \left(\frac{f_{ck}}{20}\right)^{0.25}$	τ_u = bond strength f_c' = compressive strength	S.I.
M-7 [33]	$\frac{\tau_{bu}}{\sqrt{f_c'}} = 0.77 - 0.027Xp$	τ_{bu} = bond strength (MPa), f_c' = compressive strength (MPa) Xp = corrosion %	
M-8 [34]	$\tau_{\max} = 1.22 + 3.23\left(\frac{c_{\min}}{d}\right) + 53\left(\frac{d}{l}\right)\sqrt{f_{cy}}$	$\tau_{\max}$ = bond strength, $c_{\min}$ = min. cover (25 mm), d = dia. of bar, l = embedded length	PSI
M-9 [35]	$\tau_u = \left[\left(1.06 + 2.12\left(\frac{c_{\min}}{d}\right)\right)\left(0.92 + 0.08\left(\frac{c_{\max}}{c_{\min}}\right)\right) + 75\left(\frac{d}{l}\right)\right]\sqrt{f_{cy}}$	τ_u = bond strength, $c_{\min}$ = min. cover, d = diameter of bar, $c_{\max}$ = max. cover, l = embedded length	PSI
M-10 [36]	$\tau_{\max.} = 4.9\left[\frac{\frac{c_{\min}}{d} + 0.5}{\frac{c_{\min}}{d} + 3.6}\right] f_{ct}$ $\left(\text{for } f_{cy} < 50 \text{ MPa}\right)$ $\tau_{\max.} = 8.6\left[\frac{\frac{c_{\min}}{d} + 0.5}{\frac{c_{\min}}{d} + 5.5}\right] f_{ct}$ $\left(\text{for } f_{cy} > 50 \text{ MPa}\right)$ here, $f_{ct} = 0.55\sqrt{f_{cy}}$	$\tau_{\max.}$ = ultimate bond strength, $c_{\min}$ = min. cover, d = dia. of bar, f_{ct} = tensile strength (MPa), f_{cy} = cylindrical compressive strength	S.I.
M-11 [37]	$\tau_{\max} = \left\{0.21 + 0.26\left(\frac{c_{\min}}{d}\right) + 6.32\left(\frac{d}{l}\right)\right\}\sqrt{f_c}$	$\tau_{\max}$ = bond strength, f_c = compressive strength, l = embedded length, d = dia. of bar	S.I.
M-12 [38]	$\tau_{\max} = 0.75\sqrt{f_{cy}}\left(\left(\frac{c_{\min}}{d}\right)^{\frac{2}{3}}\right)$ $\left(\text{for } f_{cy} < 48 \text{ MPa}\right)$ $\tau_{\max} = 0.95\sqrt{f_{cy}}\left(\left(\frac{c_{\min}}{d}\right)^{\frac{2}{3}}\right)$ $\left(\text{for } f_{cy} > 48 \text{ MPa}\right)$	$\tau_{\max}$ = bond strength, f_{cy} = cylindrical compressive strength, $c_{\min}$ = min. cover, d = dia. of bar	S.I.

six analytical models were selected and referred to as Group-2 (G-2). Group-1 (G-1) comprises of models M-1 to M-6, while Group-2 (G-2) consists of models M-7 to M-12, respectively. The M-6 model performed the best among those in G-1 group, securing the top rank based on performance indices. M-6 model attained an *R*-value of 0.3275 and the lowest MAE and RMSE values among the group. The MAE value of M-6 model was 41.92%,

121.83%, 202.18%, 57.64%, and 0.87% lower than that of M-1, M-2, M-3, M-4, and M-5, respectively. Similarly, the RMSE value of M-6 model was 44.20%, 109.42%, 168.47%, 58.33%, and 9.78% lower than those of M-1, M-2, M-3, M-4, and M-5 models, respectively. Additionally, M-6 model exhibited a MAPE value of 39.12%, which was 53.84%, 209.79%, 9.84%, and 3.39% lower than that of M-2, M-3, M-4, and M-5 models, respectively. However, the M-1 model had the lowest MAPE value among the models in G-1 group. The MAPE value of M-6 model was 2.53% higher than that of M-1 model. The lower error justified the superior performance of M-6 model compared to the other models in Group G-1. Furthermore, M-6 model also had the highest value of the a20-index, except for M-5 model. However, M-5 model exhibited a negative value of NS, indicating its poor performance. Additionally, within G-1 group, M-6 model attained the highest R-value, indicating a stronger correlation between experimental and predicted values.

In the G-2 context, when considering performance indices, the M-10 model emerged as the top performer within the cohort, exhibiting an impressive *R*-value of 0.3057. The M-7 model shows the highest *R*-value of 0.5435 which was 43.75% higher than the M-10 model. However, M-10 model had the lowest values of errors among the group, which shows the better performance of M-10 model in comparison to other models in G-2 group. M-10 model represents the lowest values of MAE and RMSE among G-2 group. The MAE value of M-10 model was 73.27%, 4.31%, 10.34%, 35.34% and 24.56% lower than the M-7, M-8, M-9, M-11 and M-12 models, respectively. The RMSE value of M-10 model was 3.05 MPa which was 53.11%, 0.98%, 26.88%, 26.88% and 16.06% lower than M-7, M-8, M-9, M-11 and M-12 models respectively. The M-10 model also exhibits a lower value of MAPE in comparison to M-7, M-9, M-11 and M-12 models. The MAPE value was 3.96% higher than the MAPE value of M-8 model. The M-10 model also indicate higher value of NS in comparison to M-8, M-9, M-11 and the M-12 models. M-9 and M-11 models had negative values of NS which shows the poor performance of these models among G-2 group. Therefore, from all the comparisons based on performance indices it can be concluded that M-10 model showed best performance among the G-2 group. Fig. 4 represents performance indices and graphical correlation within predicted and experimental values of all analytical models and international design guidelines. The performance of the M-6 model can be seen, as the maximum data was scattered around a linear line. Also, the scatter plot reveals the limited performance of all other existing analytical models and international design guidelines.

6.1 Discussions

From the above comparison between models of G-1 and G-2 group, the best selected models were M-6 and M-10. The M-6 model exhibited a greater *R*-value in contrast to M-10 model which was 6.65% higher. A higher *R*-value indicates a stronger linear relationship, implying that the model can effectively explain the variation in the data. In this case, M-6 model exhibited a greater *R*-value than M-10 model, signifying a higher level of explanatory power. This finding suggests that M-6 model may be better suited for linear data patterns or relationships. The MAPE value of M-10 model was 13.95% lower than the MAPE value of M-6 model. The error values i.e., MAE and RMSE values of M-6 model were lower than the M-10 model. Minimal errors shows the prediction efficiency of models. In M-6 model the MAE value was 18.77% lower than the M-10 model. Also, the RMSE value of M-6 model was 21.37% lower than the RMSE value of M-10 model. Despite M-6 model having a higher R-value, M-10 model demonstrated a lower MAPE, indicating a better overall accuracy in predicting the values. Additionally, M-6 model exhibited lower MAE and RMSE values, further highlighting its superior predictive performance in terms of minimizing errors. The M-6 model had a20-index value of 0.387 which was 41.65% higher than the M-10 model. The a20-index value measures the proportion of predictions deviating from the actual values by not more than 20%. A higher a20-index value indicates a higher proportion of accurate predictions within a certain margin of error. In this case, M-6 model had a substantially higher a20-index value compared to M-10 model, further emphasizing its superior predictive capability in terms of precision within a specific margin. Also, from performance indices, the M-6 model performed better than the M-10 model. The comparison between the two respective models is given in Table 3. Fig. 5 illustrates the comparison of mean, standard deviation (SD), and covariance (CoV) derived from the ratio of experimental to predicted values of all models. The mean ratio signifies the average deviation between the experimental values and the predictions made by each model. A lower mean ratio indicates a closer alignment between the predicted and actual values, suggesting higher accuracy. Standard deviation measures the spread or variability of the ratios around the mean.

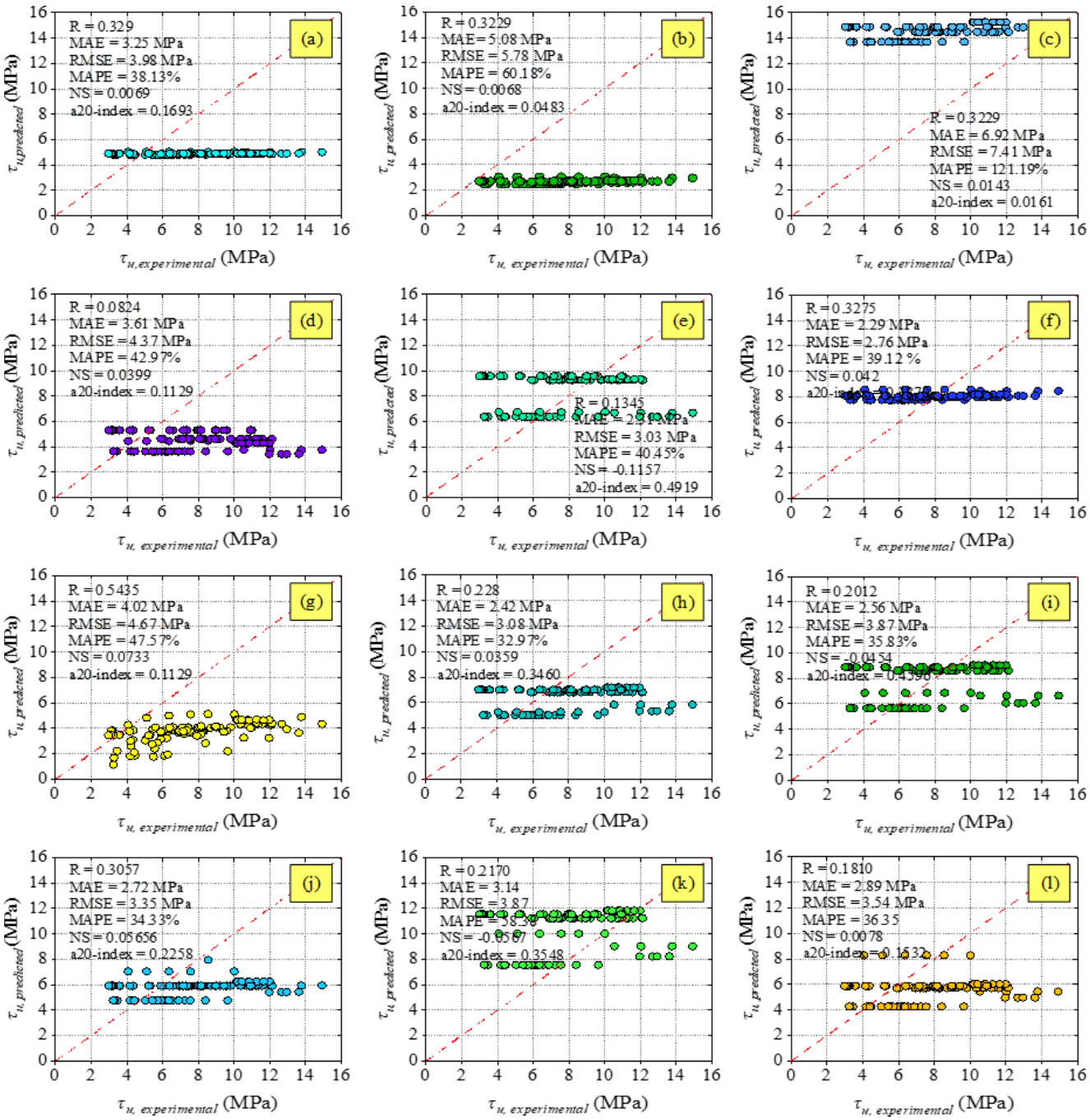

Fig. 4 Experimental vs. predicted values of testing samples: (a) M-1, (b) M-2, (c) M-3, (d) M-4, (e) M-5, (f) M-6, (g) M-7, (h) M-8, (i) M-9, (j) M-10, (k) M-11 and (l) M-12

Table 3 Comparison between two selected models in G-1 and G-2 (M-6 and M-10)

Group	Model	R	MAE (MPa)	RMSE (MPa)	MAPE (%)	NS	a20-index	CoV (pre/exp.)
Group-1	M-6	0.3275	2.29	2.76	39.12	0.042	0.387	0.4408
Group-2	M-10	0.3057	2.72	3.35	34.33	0.0565	0.2258	0.4387

A smaller standard deviation indicates more consistency in the predictions across different data points. Covariance assesses the relationship between the deviations of experimental and predicted values. A lower covariance suggests a stronger agreement between the two sets of values. Fig. 5 distinctly indicates that M-6 model exhibited a maximum number of values around 1. This observation suggested that the predicted values closely align with the

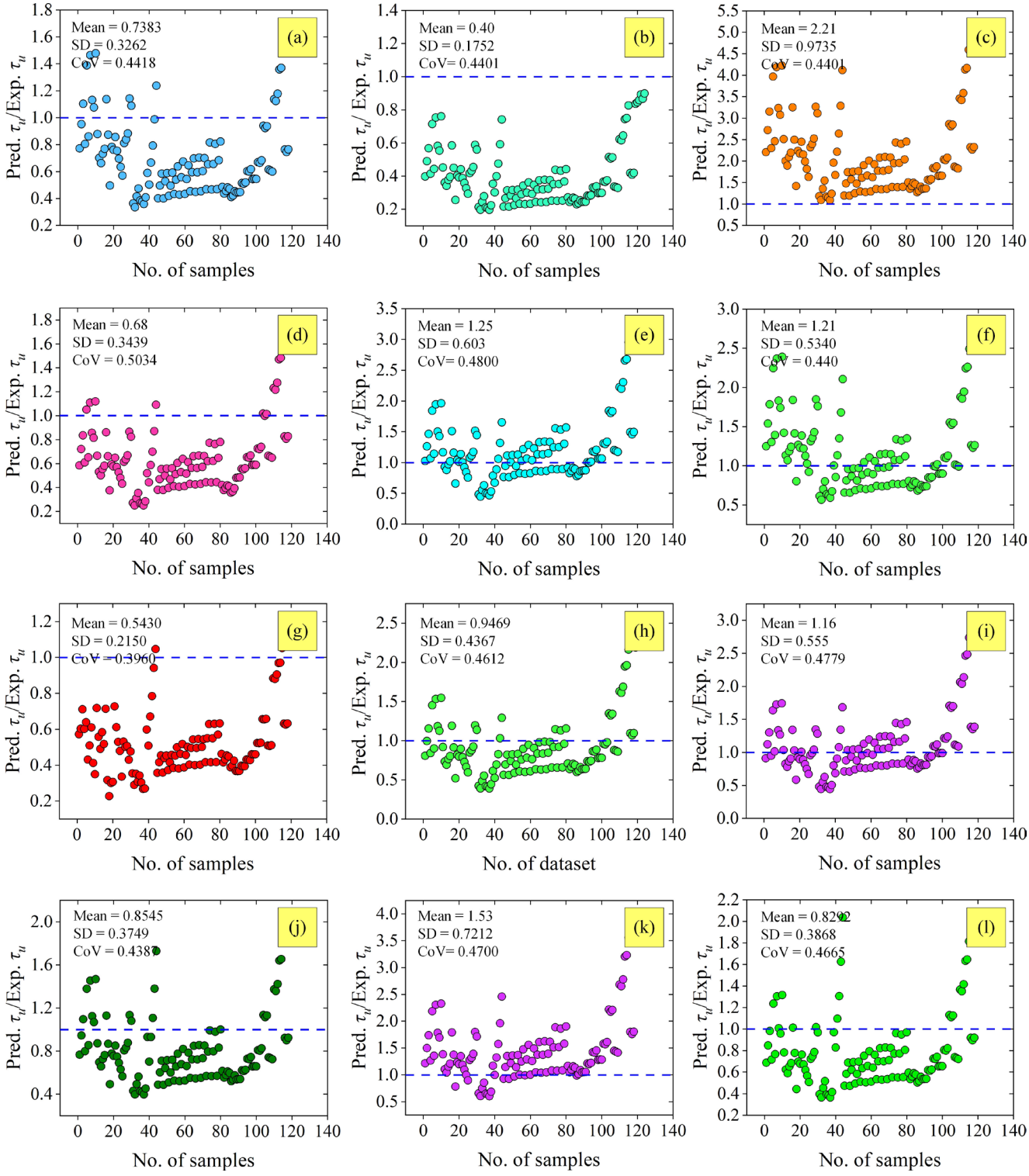

Fig. 5 Performance of analytical models and international design guidelines: (a) M-1, (b) M-2, (c) M-3, (d) M-4, (e) M-5, (f) M-6, (g) M-7, (h) M-8, (i) M-9, (j) M-10, (k) M-11 and (l) M-12

experimental ones. The performance of other models can also be seen in Fig. 5.

7 Sensitivity analysis

Sensitivity analysis was also conducted to check the influence of selected parameters on BS. This sensitivity analysis would help to understand how changes in these parameters could affect BS.

One of the key parameters examined was compressive strength (f_c'). Fig. 6 (a) revealed that an increase in f_c' led to a corresponding increase in BS. This is due to the improved interlocking effect between steel and concrete.

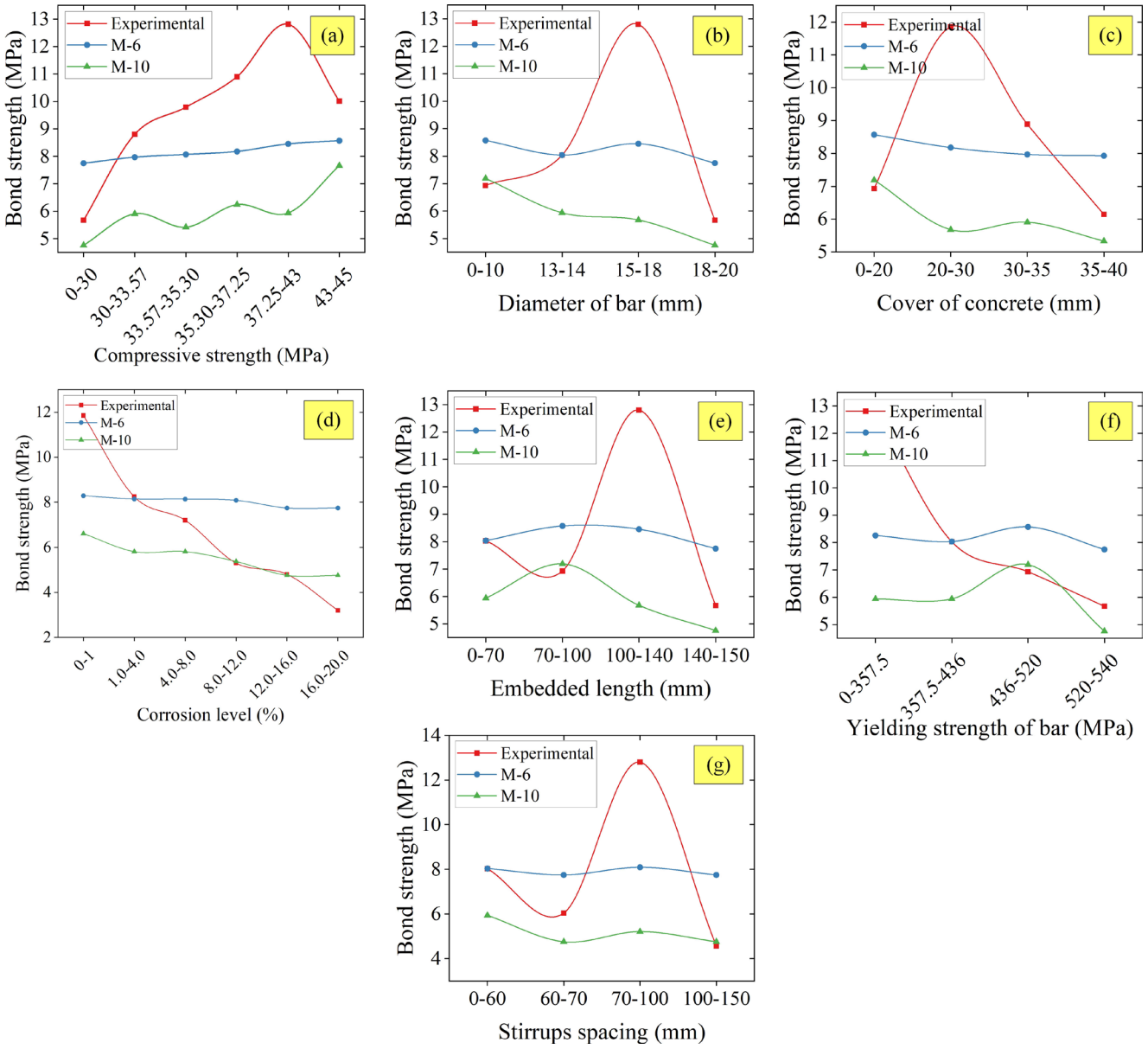

Fig. 6 Sensitivity analysis with comparison between experimental and predicted values of M-6 and M-10 models: (a) Compressive strength of concrete; (b) Diameter of bar; (c) Cover of concrete; (d) Corrosion level; (e) Embedded length; (f) Yield strength of bar; (g) Stirrups spacing

The higher grade of concrete provides more confinement as compared to the lower grade. Similar results had been concluded by Xuan et al. [39].

The second important parameter analysed was the diameter of bar (d_b). Fig. 6 (b) showed that larger bar diameters resulted in lower BS. The reason attributed to this was reduced contact area between the steel and concrete for larger bars which was because of the smaller surface area to volume ratio of larger diameter bars. Similar results had been concluded by Shunmuga Vembu and Ammasi [40], Krishnaveni and Rajendran [41].

The third parameter analysed was the cover of concrete (c). Fig. 6 (c) showed that thicker cover could enhance BS because of better confinement to steel reinforcement. The results coincide with the findings of Shunmuga Vembu and Ammasi [40].

Another important parameter was corrosion level (η). The Fig. 6 (d) revealed that with the increased corrosion percentage the BS decreases. This was due to a decrease in the diameter and yield strength of the bar.

From Fig. 6 (e) it was clear that with an increase in l_b the BS decreases. This was because of non-uniform stress distribution along the length of the bar. Similar results related to corrosion level and development length of rebar were discussed by Shunmuga Vembu and Ammasi [40], Krishnaveni and Rajendran [41].

The remaining parameters analysed were stirrups spacing and the yield strength of the bar. From Fig. 6 (f) and (g) it was clear that with the increase in yield strength and stirrups spacing BS decreases. Wider spacing leads to weaker BS. A similar result was concluded by Shunmuga Vembu and Ammasi in their findings [40], while the steel bars considered in this study were corroded, so with an increase in f_y, BS decreases. Fig. 6 shows the comparison between experimental values and predicted values by M-6 and M-10 models.

8 Conclusions

In this study, a comparison was made among analytical models and international design guidelines to check the precision of the given models by validating them through the collected dataset. The dataset comprises of experimental observations, with parameters including l_b, η, d_b, t_b, f_c', c, f_y, S_v and S_d. Through analysis of the results, the following conclusions were drawn:

- For better comparison, the selected models were divided into two groups which were G-1 and G-2. From these two groups, M-6 model (G-1) and M-10 model (G-2) performed best on the basis of performance indices.
- The R-value of M-6 model was 0.3275, indicating a 6.65% increase compared to the M-10 model with a value of 0.3057. Additionally, M-6 model exhibited lower MAE and RMSE values than M-10 model, with a reduction of 18.77% and 21.37%, respectively. The a20-index value of M-6 model was 41.65% higher than the M-10 model.
- Based on performance indices it can be concluded that M-6 model had better accuracy in predicting the BS based on the beam test.
- Sensitivity analysis results showed that with the increase in f_c' and c, BS increases and with an increase in η, d_b and l_b, the BS decreases.

8.1 Limitations

Increasing the number of datasets may enhance the accuracy of the existing models. Furthermore, the study's accuracy is influenced by the limited consideration of analytical and international design guidelines. Expanding the scope to include more design guidelines and analytical models could contribute to a more comprehensive and accurate evaluation.

8.2 Future scope

In the future, better outcomes may be generated by incorporating a large number of datasets and considering a greater number of design guidelines and analytical models from the literature, thus improving the accuracy of predicted results. Additionally, considering ML models could contribute to more relevant results. The failure pattern prediction along with BS prediction could increase the applicability of the developed ML model.

Nomenclature

RC	Reinforced concrete
HBT	Hinge beam test
BS	Bond strength
R	Coefficient of correlation
MAPE	Mean absolute percentage error
RMSE	Root mean square error
NS	Nash-Sutcliffe eff. index
MAE	Mean absolute error
CoV	Covariance
SD	Standard deviation
c	Cover
d_b	Diameter of bar
t_b	Type of bar
l_b	Development length
f_c'	Compressive strength
f_y	Yield strength of bar
S_v	Stirrups spacing
S_d	Stirrup diameter
τ_u	Bond strength
ANFIS	Adaptive neuro-fuzzy inference system
ANN	Artificial neural network
GEP	Gene expression programming
MOGA-EPR	Multi-objective genetic algorithm evolutionary polynomial regression
TRM	Textile reinforced mortars
ABC-ANN	Artificial bee colony optimization algorithm
SRG	Steel reinforced grout

References

[1] Li, Z., Qi, J., Hu, Y., Wang, J. "Estimation of bond strength between UHPC and reinforcing bars using machine learning approaches", Engineering Structures, 262, 114311, 2022. https://doi.org/10.1016/j.engstruct.2022.114311

[2] Güneyisi, E. M., Mermerdaş, K., Gültekin, A. "Evaluation and modeling of ultimate bond strength of corroded reinforcement in reinforced concrete elements", Materials and Structures, 49(8), pp. 3195–3215, 2016. https://doi.org/10.1617/s11527-015-0713-4

[3] Ma, Y., Guo, Z., Wang, L., Zhang, J. "Experimental investigation of corrosion effect on bond behavior between reinforcing bar and concrete", Construction and Building Materials, 152, pp. 240–249, 2017. https://doi.org/10.1016/j.conbuildmat.2017.06.169

[4] Singh, R., Arora, H. C., Bahrami, A., Kumar, A., Kapoor, N. R., Kumar, K., Rai, H. S. "Enhancing Sustainability of Corroded RC Structures: Estimating Steel-to-Concrete Bond Strength with ANN and SVM Algorithms", Materials, 15(23), 8295, 2022. https://doi.org/10.3390/ma15238295

[5] Cavaleri, L., Barkhordari, M. S., Repapis, C. C., Armaghani, D. J., Ulrikh, D. V., Asteris, P. G. "Convolution-based ensemble learning algorithms to estimate the bond strength of the corroded reinforced concrete", Construction and Building Materials, 359, 129504, 2022. https://doi.org/10.1016/j.conbuildmat.2022.129504

[6] Yalciner, H., Eren, O., Sensoy, S. "An experimental study on the bond strength between reinforcement bars and concrete as a function of concrete cover, strength and corrosion level", Cement and Concrete Research, 42(5), pp. 643–655, 2012. https://doi.org/10.1016/j.cemconres.2012.01.003

[7] Chai, X., Shang, H., Zhang, C. "Bond behavior between corroded steel bar and concrete under sustained load", Construction and Building Materials, 310, 125122, 2021. https://doi.org/10.1016/j.conbuildmat.2021.125122

[8] Cabrera, J. G. "Deterioration of concrete due to reinforcement steel corrosion", Cement and Concrete Composites, 18(1), pp. 47–59, 1996. https://doi.org/10.1016/0958-9465(95)00043-7

[9] Yalciner, H., Marar, K. "Experimental Study on the Bond Strength of Different Geometries of Corroded and Uncorroded Reinforcement Bars", Journal of Materials in Civil Engineering, 29(7), 05017002, 2017. https://doi.org/10.1061/(ASCE)MT.1943-5533.0001914

[10] Mousavi, S. S., Dehestani, M., Mousavi, K. K. "Bond strength and development length of steel bar in unconfined self-consolidating concrete", Engineering Structures, 131, pp. 587–598, 2017. https://doi.org/10.1016/j.engstruct.2016.10.029

[11] Almusallam, A. A., Al-Gahtani, A. S., Aziz, A. R., Rasheeduzzafar "Effect of reinforcement corrosion on bond strength", Construction and Building Materials, 10(2), pp. 123–129, 1996. https://doi.org/10.1016/0950-0618(95)00077-1

[12] Choi, Y. S., Yi, S.-T., Kim, M. Y., Jung, W. Y., Yang, E. I. "Effect of corrosion method of the reinforcing bar on bond characteristics in reinforced concrete specimens", Construction and Building Materials, 54, pp. 180–189, 2014. https://doi.org/10.1016/j.conbuildmat.2013.12.065

[13] Lin, H., Zhao, Y. "Effects of confinements on the bond strength between concrete and corroded steel bars", Construction and Building Materials, 118, pp. 127–138, 2016. https://doi.org/10.1016/j.conbuildmat.2016.05.040

[14] Zhao, Y., Lin, H., Wu, K., Jin, W. "Bond behaviour of normal/recycled concrete and corroded steel bars", Construction and Building Materials, 48, pp. 348–359, 2013. https://doi.org/10.1016/j.conbuildmat.2013.06.091

[15] Mangat, P. S., Elgarf, M. S. "Bond characteristics of corroding reinforcement in concrete beams", Materials and Structures, 32(2), pp. 88–97, 1999. https://doi.org/10.1007/BF02479434

[16] Shang, H., Zhou, J., Fan, G., Yang, G., You, W. "Study on the bond behavior of steel bars embedded in concrete under the coupling of sustained loads and chloride ion erosion", Construction and Building Materials, 276, 121684, 2021. https://doi.org/10.1016/j.conbuildmat.2020.121684

[17] Shang, H., Chai, X. "Bond behavior between corroded steel bar and concrete under reciprocating loading history of beam type specimens", Engineering Structures, 247, 113112, 2021. https://doi.org/10.1016/j.engstruct.2021.113112

[18] Hou, L., Liu, H., Xu, S., Zhuang, N., Chen, D. "Effect of corrosion on bond behaviors of rebar embedded in ultra-high toughness cementitious composite", Construction and Building Materials, 138, pp. 141–150, 2017. https://doi.org/10.1016/j.conbuildmat.2017.02.008

[19] Shbeeb, N. I., Katash, A. A., Oguzmert, M., Barham, W. S. "Estimation of the Bond Strength of Fiber-Reinforced Polymer Bars in Concrete Using Artificial Intelligence Systems", Buildings, 14(2), 369, 2024. https://doi.org/10.3390/buildings14020369

[20] Jahangir, H., Nikkhah, Z., Rezazadeh Eidgahee, D., Esfahani, M. R. "Performance based review and fine-tuning of TRM-concrete bond strength existing models", Journal of Soft Computing in Civil Engineering, 7(1), pp. 43–55, 2023. https://doi.org/10.22115/SCCE.2022.349483.1476

[21] Al-Hamd, R. K. S., Albostami, A. S., Alzabeebee, S., Al-Bander, B. "An optimized prediction of FRP bars in concrete bond strength employing soft computing techniques", Journal of Building Engineering, 86, 108883, 2024. https://doi.org/10.1016/j.jobe.2024.108883

[22] Jahangir, H., Rezazadeh Eidgahee, D., Esfahani, M. R. "Bond strength characterization and estimation of steel fibre reinforced polymer-concrete composites", Steel and Composite Structures, 44(6), pp. 803–816, 2022. https://doi.org/10.12989/scs.2022.44.6.803

[23] Jahangir, H., Rezazadeh Eidgahee, D. "A new and robust hybrid artificial bee colony algorithm – ANN model for FRP-concrete bond strength evaluation", Composite Structures, 257, 113160, 2021. https://doi.org/10.1016/j.compstruct.2020.113160

[24] Jahangir, H., Esfahani, M. R. "Investigating loading rate and fibre densities influence on SRG - concrete bond behaviour", Steel and Composite Structures, 34(6), pp. 877–889, 2020. https://doi.org/10.12989/scs.2020.34.6.877

[25] Jahangir, H., Soleymani, A., Esfahani, M. R. "Investigating the Confining Effect of Steel Reinforced Polymer and Grout Composites on Compressive Behavior of Square Concrete Columns", Iranian Journal of Science and Technology, Transactions of Civil Engineering, 47(2), pp.775–791, 2023. https://doi.org/10.1007/s40996-022-00917-7

[26] Kumar, A., Arora, H. C., Kapoor, N. R., Kumar, K. "Prognosis of compressive strength of fly-ash-based geopolymer-modified sustainable concrete with ML algorithms", Structural Concrete: Journal of the fib, 24(3), pp. 3990–4014, 2023. https://doi.org/10.1002/suco.202200344

[27] Kumar, K., Saini, R. P. "Adaptive neuro-fuzzy interface system-based performance monitoring technique for hydropower plants", ISH Journal of Hydraulic Engineering, 29(5), pp. 611–621, 2023. https://doi.org/10.1080/09715010.2022.2115320

[28] Kumar, A., Arora, H. C., Kapoor, N. R., Mohammed, M. A., Kumar, K., Majumdar, A., Thinnukool, O. "Compressive Strength Prediction of Lightweight Concrete: Machine Learning Models", Sustainability, 14(4), 2404, 2022. https://doi.org/10.3390/su14042404

[29] Comité Euro-International du Béton "CEB-FIP model code 1990: Design code", Thomas Telford Publishing, 1990. ISBN 0727739441

[30] Taerwe, L., Matthys, S. "Fib model code for concrete structures 2010", Ernst & Sohn, Wiley, 2013. ISBN 9783433604090 [online] Available at: http://hdl.handle.net/1854/LU-4255771 [Accessed: 13 March 2024]

[31] Chowdhury, S. H., Loo, Y. C. "Complexities and Effectiveness of Australian Standard for Concrete Structures — As 3600-2018", In: EASEC16: Proceedings of The 16th East Asian-Pacific Conference on Structural Engineering and Construction, Brisbane, Australia, 2019, pp. 1747–1756. ISBN 978-981-15-8078-9 https://doi.org/10.1007/978-981-15-8079-6_161

[32] Allen, J. H., Azizinamini, A., Balazs, G. L., Browning, J., Cox, J. V., DeVries, R. A., …, Zuo, J. "Bond and Development of Straight Reinforcing Bars in Tension", American Concrete Institute, Detroit, MI, USA, Rep. ACI 408R-03, 2003.

[33] Stanish, K. D., Hooton, R. D., Pantazopoulou, S. J. "Corrosion effects on bond strength in reinforced concrete", ACI Structural Journal, 96(6), pp. 915–921, 1999.

[34] Orangun, C. O., Jirsa, J. O., Breen, J. E. "A re-evaluation of test data on development length and splices", ACI Structural Journal, 74(3), pp. 114–122, 1977.

[35] Darwin, D., McCabe, S. L., Idun, E. K., Schoenekase, S. P. "Development length criteria. Bars not confined by transverse reinforcement", ACI Structural Journal, 89(6), pp. 709–720, 1992.

[36] Esfahani, M. R., Rangan, B. V. "Local bond strength of reinforcing bars in normal strength and high-strength concrete (HSC)", ACI Structural Journal, 95(2), pp. 96–106, 1998.

[37] Siempu, R., Pancharthi, R. K. "Bond characteristics of concrete made of recycled aggregates from building demolition waste", Magazine of Concrete Research, 69(13), pp. 665–682, 2017. https://doi.org/10.1680/jmacr.16.00400

[38] Harajli, M. H. "Comparison of Bond Strength of Steel Bars in Normal- and High-Strength Concrete", Journal of Materials in Civil Engineering, 16(4), pp. 365–374, 2004. https://doi.org/10.1061/(ASCE)0899-1561(2004)16:4(365)

[39] Xuan, V. T., Manh, H. N., Trung, H. N., Xuan, D. P. "Experimental Study on the Bond Strength Between Reinforcement Bars and Concrete as a Function of Concrete Strength and Confinement Effect", In: CIGOS 2021, Emerging Technologies and Applications for Green Infrastructure: Proceedings of the 6th International Conference on Geotechnics, Civil Engineering and Structures, Ha Long, Vietnam, 2022, pp. 257–263. ISBN 978-981-16-7159-3 https://doi.org/10.1007/978-981-16-7160-9_25

[40] Shunmuga Vembu, P. R., Ammasi, A. K. "A Comprehensive Review on the Factors Affecting Bond Strength in Concrete", Buildings, 13(3), 577, 2023. https://doi.org/10.3390/buildings13030577

[41] Krishnaveni, S., Rajendran, S. "A state of the art on characterization and application of artificial neural networks on bond strength between steel rebar and concrete", Construction and Building Materials, 354, 129124, 2022. https://doi.org/10.1016/j.conbuildmat.2022.129124

Appendix A

Table A1 Dataset details

S. No.	References	No. of specimen	Input parameters									Output
			f_c' (MPa)	l_b (mm)	d_b (mm)	t_b	f_y (MPa)	c (mm)	η (%)	S_v (mm)	S_d (mm)	τu (MPa)
1	[13]	30	30	150	20	1	540	40	1.01–20.86	70–150	6	3.24–9.64
2	[14]	8	35.3–42.5	140	18	1	357.5	30	0.78–10.04	100	8	10.54–14.92
3	[15]	6	45	100	10	2	520	20	0.3–5	–	–	4.07–10.01
4	[7]	36	33.57	70	14	2	436	35	0.71–4.67	60	6	5.9–12.12
5	[16]	8	37.25	70	14	2	436	30	0.08–0.53	60	6	10.13–11.97
6	[17]	36	35.43	70	14	2	436	40	2.58–7.42	60	6	2.98–11